

Wideband pulse propagation: single-field and multi-field approaches to Raman interactions

P. Kinsler and G.H.C. New

Department of Physics, Imperial College London, Prince Consort Road, London SW7 2BW, United Kingdom.

(Dated: September 20, 2018)

We model the process of ultra broadband light generation in which a pair of laser pulses separated by the Raman frequency drive a Raman transition. In contrast to the usual approach using separate field envelopes for the different frequency components, we treat the field as a single entity. This requires the inclusion of few-cycle corrections to the pulse propagation. Our single-field model makes fewer approximations and is mathematically (and hence computationally) simpler, although it does require greater computational resources to implement. The single-field theory reduces to the traditional multi-field one using appropriate approximations.

PACS numbers: 42.65.Re,42.50.Gy,31.15.-p

Published as Phys. Rev. A72, 033804 (2005). A detailed derivation of the single-field theory can be found at <http://arxiv.org/abs/physics/0606112>

I. INTRODUCTION

An important aim of current wideband Raman experiments is to efficiently generate few-cycle pulses [1, 2, 3, 4]. If driven strongly enough, the two-photon Raman transition modulates the incoming field by adding sidebands separated by the transition frequency. Wideband fields are generated as these sidebands generate sidebands of their own (and so on); a wide comb of frequency components separated by the transition frequency is generated in this way. If a scheme can be implemented that adjusts the phases of each component appropriately, then few- or single- cycle optical pulses can be obtained (see e.g. [2]).

In standard theoretical treatments of the Raman process, the field is split into frequency components centred on the teeth of the frequency comb. This approach has the advantage that the components can be modeled reasonably well with slowly varying envelopes, but of course it has the disadvantage that one needs to keep track of a large number of components. In this paper, we study an alternative approach in which the field is treated as a single entity rather than being split into pieces. Note that this approach is distinct from methods based on the direct solution of Maxwell's equations such as FDTD (finite difference time domain)[5] or PSSD (pseudospectral spatial domain)[6]. Our single-field is based on a second-order wave equation, and uses a convenient choice of carrier to define a field envelope. As we will demonstrate, the latter technique offers significant advantages over the traditional multi-field formalism.

To provide a context for the discussion, we consider experiments such as those of Sali et.al. [4, 7], where the Raman transition is driven near-resonantly by a pair of intense pump pulses about 100fs long; compared to the transition frequency of about 130THz, the spectra of each pump pulse (and hence the generated sidebands) are relatively narrow. This means that a multi-component model is still not unreasonable, even if numerical considerations might demand that the arrays used to store these spectra overlap in frequency space. However, if we were to move to shorter pump pulses, or to a single (much

shorter) pump pulse with enough bandwidth to efficiently excite the transition, we would reach the regime where the teeth of the frequency comb significantly overlap. At this point, one would be forced not only to move from a solution based on the Slowly-Varying Envelope Approximation (SVEA) to a more accurate model such as the Generalized Few-Cycle Envelope Approximation (GFEA) [8, 9], but the utility of multiple field components would in any case become questionable. This provides the motivation for the present work, since our model can extend the regime in which the advantages of envelope-based methods can be utilised; it also turns out to be more versatile, placing fewer restrictions on the kinds of Raman media that can be easily described.

In this paper, we will construct a single-field model which, in most other respects, closely parallels the approach to wideband Raman generation adopted by Hickman et. al. [10]. A key feature of the single-field model is that the coupling constants oscillate at the Raman frequency, and it is this that impresses the sideband modulation on the propagating field. Since the field is now not only wide-band but contains significant sideband components (i.e. distinct sub-peaks, as opposed to a broad featureless background), the field envelope is no longer slowly-varying and must therefore be propagated using the GFEA. This necessity can be demonstrated by comparing the results of the single-field model with those of a multi-field counterpart.

The paper is organized as follows: section II outlines the derivation of the single-field Raman theory, section III shows how to reduce it to a standard multi-field version, and section IV applies the theory to practical situations. In section V we discuss some of the issues relating to our Raman model and its numerical implementation, and finally section VI contains our conclusions.

II. SINGLE-FIELD RAMAN THEORY

We start by considering the wave function ψ of a single molecule (e.g. H_2) and the electric field E , and write the time-dependent wave function by expanding it in terms of the eigenfunctions in the field-free (i.e. $E = 0$) case. This means we can get the expansion coefficients by solving for an effective Schrödinger equation that contains a two-photon Rabi frequency created by means of an interaction term based on

a field-dependent dipole moment. We assume a dispersionless medium and write all equations in terms of position z and retarded times $t = t_{lab} - z/c$. Here we follow the method of Hickman, Paisner, and Bischel [10] (HPB), but we use only a single E field rather than multiple components. Note that HPB use *Gaussian* units, so there may appear to be inconsistencies when comparing our formulae (in S.I.) to theirs.

We denote the known molecular eigenfunctions of the unperturbed Hamiltonian H_0 as $|n\rangle$, and their corresponding energies $\hbar W_n$. We want to obtain the solution to

$$(H_0 + V)\psi = i\hbar \frac{\partial \psi}{\partial t}, \quad (1)$$

$$\text{with } V = -dE, \quad (2)$$

$$\psi = \sum_n c_n e^{-iW_n t} |n\rangle, \quad (3)$$

where d is the electronic dipole moment operator and the c_n are a set of complex probability amplitudes.

We now replace the electric field E with a carrier-envelope description, but, unlike HPB, we use only a single component centred at a frequency of ω_0 , rather than a set indexed by an integer j . The envelope and carrier for the field is:

$$E = A e^{-i(\omega_0 t - k_0 z)} + \text{c.c.}, \quad (4)$$

and, following the standard procedure of assuming the coefficients c_i are slowly varying, discarding terms at multiples of the carrier frequency, and simplifying, we eventually reach

$$i\hbar \frac{dc_n}{dt} = -\sum_j c_j \alpha_{nj} \cdot 2|A|^2, \quad (5)$$

$$\text{where } \alpha_{nj} = \frac{1}{\hbar} \exp[-iW_{jn}t] \sum_i d_{ni} d_{ij} \frac{W_{ij}}{W_{ij}^2 - \omega_0^2}. \quad (6)$$

The α_{nj} coupling parameters oscillate because, in contrast to the HPB derivation, there is no frequency difference between field components to cancel with the Raman transition frequency. We now take the indices 1 and 2 to correspond to the two states involved in the Raman transition of interest; these will be the 0 and 1 vibrational (or perhaps rotational) levels of the electronic ground state. Indices 3 and above will correspond to (quoting HPB) “translational motion on higher electronic states”. Since we are interested only in the Raman transition, we specialize the above equations for the coefficients c_n , calculating c_1 and c_2 only, and assuming that the $d_{12} = \langle 1|d|2\rangle$ dipole moment is zero. This means we will only be including transitions between indices 1 and 2 that *go via one of the higher states* $j \geq 3$, since we still allow $d_{1j}, d_{2j} \neq 0 \forall j \geq 3$. Further, we solve for the coefficients for the higher states in terms of c_1 and c_2 , in an adiabatic approximation justified when c_1 and c_2 vary only slowly compared to the exponential terms.

When converting the equations for c_1, c_2 into Bloch equations, we make the same approximations as HPB: keeping the energy separations for all transitions greater than that of the $1 \leftrightarrow 2$ transition, and ignoring all the higher vibrational (or rotational) states. Thus we can write

$$\alpha_{12}^* - \alpha_{21} \approx 0, \quad (7)$$

$$\alpha_{12} + \alpha_{21}^* = 2\hbar f' e^{-i\omega_b t + i\delta'}. \quad (8)$$

Here ω_b is the Raman transition frequency, and δ' is a phase factor that ensures that the coupling constant f' is real valued. This f' will be used to replace $\alpha_{12} + \alpha_{21}^*$. We also get a Stark shift term –

$$\hbar g' = \alpha_{11}^* - \alpha_{22}^*. \quad (9)$$

We define $\rho_{12} = c_1 c_2^*$ and $w = c_2^* c_2 - c_1^* c_1$, so that

$$\frac{d\rho_{12}}{dt} = i \frac{(\alpha_{11} - \alpha_{22}^*)}{\hbar} 2|A|^2 \rho_{12} + i \frac{\alpha_{12}}{\hbar} 2|A|^2 w, \quad (10)$$

$$\frac{dw}{dt} = +i \frac{2\alpha_{12}^*}{\hbar} 2|A|^2 \rho_{12} - i \frac{2\alpha_{12}}{\hbar} 2|A|^2 \rho_{12}^*. \quad (11)$$

Finally, we insert decay terms γ_i , and introduce $\omega'_b = \omega_b - \Delta$. This Δ allows for arbitrary rotations of the polarization, $\rho_{12} = \rho'_{12} \exp(-i\Delta t - i\delta')$. Eqns. (10,11) governing the response of the medium to the applied fields now become

$$\begin{aligned} \partial_t \rho'_{12} &= (-\gamma_2 + i\Delta) \rho'_{12} \\ &\quad + i g' 2A^* A \rho'_{12} + i f' 2A^* A w e^{i\omega'_b t}, \end{aligned} \quad (12)$$

$$\begin{aligned} \partial_t w &= -\gamma_1 (w' - w_i) \\ &\quad + 2i f' \cdot 2A^* A (\rho'_{12} e^{i\omega'_b t} - \rho_{12}^* e^{-i\omega'_b t}). \end{aligned} \quad (13)$$

The parameter Δ should be chosen to optimise computational accuracy by making the dynamics as slowly-varying as possible. For example, if the field contained two frequency components that were slightly detuned from the Raman frequency, we might use Δ to compensate for the resultant beating. In general, Δ is most useful in the multi-field model discussed in the next section. The complementary part that specifies how the field responds to the polarization of the Raman transition, is

$$\partial_z A(t) = \frac{2i\pi\omega_0}{c_0 n_0} \times \left[1 + \frac{i\partial_t}{\omega_0} \right] \frac{\mathcal{B}(t)}{4\pi\epsilon_0} \quad (14)$$

$$= i \frac{2\sigma\tilde{\alpha}_{12}\omega_0}{c_0 n_0 \epsilon_0} \times \left[1 + \frac{i\partial_t}{\omega_0} \right] A(t) X(t), \quad (15)$$

$$X(t) = \rho'_{12} e^{i\omega'_b t} + \rho_{12}^* e^{-i\omega'_b t}. \quad (16)$$

Here the $1 + i\partial_t/\omega_0$ in eqn.(15) is (with $\partial_t \equiv d/dt$) the lowest-order approximation to the GFEA few-cycle propagation corrections [8, 9], which is equivalent to the SEWA (Slowly Evolving Wave Approximation) correction derived by Brabec and Krausz [11]. Although the full form is not included for reasons of brevity, it could easily be introduced if the extra accuracy was desired; indeed we routinely use it in our simulation codes. It is independent of the Raman derivation presented here, since it is a field propagation effect. The full form of the few-cycle prefactor (and various expansions thereof) has already been reported in [8, 9].

A detailed derivation of this single-field Raman theory can be found in [12]

We solve these equations numerically using a split step method, where we treat the nonlinearity in the time domain, and the dispersion in the frequency domain. To include dispersion in a time domain equation like eqn.(15) requires either additional time derivatives (as in [8, 9]) or a convolution over a time-response function which is an N^2 operation.

However, handling dispersion in the frequency domain is both conceptually simpler (since it simply amounts to a frequency-dependent phase evolution), and more computationally efficient because it is an $N \log N$ process.

The validity of the approximations used in deriving our Bloch equations will obviously depend both on the details of the chosen Raman medium and/or transition, and on the number of Stokes and anti-Stokes sidebands we wish to describe. Since in the experiments of [1, 2, 3, 4, 13] the emphasis was on a single Raman transition, a simple Bloch model is clearly appropriate, and indeed our approximations differ little from those of other theoretical approaches (such as that of HPB).

III. MULTI-FIELD RAMAN THEORY

The single-field Raman model can be converted into a traditional multi-field model as developed in e.g. HPB [10] or Syed, McDonald and New [15] by replacing the field envelope with a sum of multiple envelopes using carrier exponentials spaced at the Raman frequency. When doing this, we will only get the correct multi-field form if few-cycle (either SEWA or GFEA) corrections to the field evolution part of the theory are applied to the effective polarization caused by the Raman transition.

Since the single-field evolution equation (eqn.(15)) uses an envelope A that is based on a carrier (see eqn.(4)), the single-field envelope A is replaced with A_j 's at frequency $\omega_j = \omega_0 + j\omega_b$ and wavevector $k_j = k(\omega_j)$. The single-field envelope in terms of the new A_j 's is

$$A = \sum_j A_j \exp[-i(\omega'_j t - k'_j z)], \quad (17)$$

where $\omega'_j = \omega_j - \omega_0$, and $k'_j = k_j - k(\omega_0) = k_j - k_0$.

The equations for ρ'_{12} and w describing the Raman transition result from a simple substitution of eqn.(17) into eqns.(12, 13), followed by a rotating wave approximation (RWA) to remove non frequency matched terms. They are

$$\begin{aligned} \partial_t \rho'_{12} \approx & \left(-\gamma_2 + i\Delta + ig' \sum_j 2A_j^* A_j \right) \rho'_{12} \\ & + 2if' \sum_j 2A_j A_{j-1}^* w e^{-i\Delta t} \cdot e^{+i(k_j - k_{j-1})z}, \quad (18) \end{aligned}$$

$$\begin{aligned} \partial_t w = & -\gamma_1 (w - w_i), \\ & + 2if' \left(2A_j^* A_{j+1} \rho'_{12} e^{i\omega_b t} - 2A_j A_{j+1}^* \rho'_{12} e^{-i\omega_b t} \right). \quad (19) \end{aligned}$$

Quite a lot of physics has been removed by the RWA approximation, although it is a very reasonable one except in the very wideband limit. For example, the effects of next-nearest neighbour field components have been ignored, as have all more distant field-field interactions. In the next-nearest neighbour case, the dropped terms would impose a rapid ω_b oscillation onto the polarization ρ_{12} , which would in turn tend to impose sidebands at $\pm\omega_b$ onto each field component. It is reasonable to ignore such sidebands in the narrowband limit used for most applications of a multi-field Raman theory; but,

in principle one might extend a multi-field theory to include them by inventing a scheme to apply the sidebands to the field component with which they are in nearest resonance.

Extra factors of 2 have appeared in eqns.(18, 19) because the multi-field equations start with double summations that give pairs of terms that can be reduced to one in the remaining single summation.

Finally, we need to insert the few-cycle correction to the polarization term, because the ($j \neq 0$) sub-envelopes A_j have an $i j \omega_b t$ time dependence that cannot be neglected. The polarization correction terms are just the result of applying the first-order correction ($i/\omega_0 \partial_t$) to the $A(t)X(t)$ from eqn.(15). The j -th polarization correction term is then

$$\begin{aligned} & i \frac{\sigma \omega'_j \alpha_{12}}{2\epsilon_0 c_0} \left\{ \rho'_{12} A_{j+1} \exp[+i(k'_{j+1} - k'_j)z - i\Delta t] \right. \\ & \quad \left. + \rho_{12}^* A_{j-1} \exp[+i(k'_{j-1} - k'_j)z + i\Delta t] \right\} \\ & - i(k_j - k_0) A_j, \quad (20) \end{aligned}$$

and differs only from the standard polarization term in that ω'_j appears in place of ω_0 . The two terms can then be straightforwardly summed, and since $\omega_j = \omega_0 + \omega'_j$, from eqns.(15, 16, 17), we get

$$\begin{aligned} \partial_z A_j(t) = & i \frac{\sigma \omega_j \alpha_{12}}{2\epsilon_0 c_0} \left\{ \rho'_{12} A_{j+1} \exp[+i(k'_{j+1} - k'_j)z - i\Delta t] \right. \\ & \quad \left. + \rho_{12}^* A_{j-1} \exp[+i(k'_{j-1} - k'_j)z + i\Delta t] \right\} \\ & - i(k_j - k_0) A_j, \quad (21) \end{aligned}$$

where the $i\Delta t$ terms arise because of our rotation of the frame of reference of ρ'_{12} . The residual $k_j - k_0$ terms result from a difference in the k frame of reference between the our multi-field derivation and the standard one.

IV. EXAMPLE APPLICATIONS

We now use the single-field (GFEA) model to simulate an experimental situation. First we compare the results to their multi-field counterparts, demonstrating the relationships between the two methods, and showing them to be in good agreement, as expected for the chosen pulse lengths. Second, we contrast our model with an (inaccurate) single-field SVEA model, in order to highlight the role of the few-cycle propagation terms. The bulk of the code used was the same for all simulations, as it contains options to switch from a single to a multi-field case, and to switch GFEA corrections on and off.

Figure 1 shows a set of results for a pair of pump pulses traveling though 9cm of H_2 . This corresponds to a simulation of an experiment where the pulses pump the 1st vib(ro) level in molecular H_2 (at 4155cm^{-1} , i.e. $\sim 126\text{THz}$), as in the transient-regime experiments of Sali et al. [4, 7]. In these experiments, typical pulses might be 70fs and 250fs wide at 800nm ($30\mu\text{J}$) and 600nm ($120\mu\text{J}$) respectively, and the comb of Raman sidebands generated are narrow and well separated. A Cauchy-type dispersion curve for H_2 is incorporated into the simulations. In our simulations, we use the smaller widths of 17.5fs and 62.5fs, which broadens the spectral peaks (to

about 57THz and 16THz respectively) and makes the standard multi-field approach less practical. The figure compares three data sets – (a) single-field GFEA simulation, (b) multi-field simulation, and lastly (c) single-field SVEA simulation (i.e. *without* any few-cycle propagation corrections).

There is good agreement in the heights of all the spectral peaks between the two exact simulations (single-field GFEA fig. 1(a) and multi-field fig 1(b)); even the details in the wings of the first anti-Stokes peak (at about $f = 0.5$) are replicated. Those in the wings of the second anti-Stokes peak (at about $f = 0.63$) are not well replicated; however, the features in question are about three orders of magnitude weaker than the peaks, and the two simulations are not equivalent because the multi-field theory does not include next-nearest neighbour interactions.

The comparison between fig. 1(a,b) and the single-field SVEA simulation fig 1(c) is also instructive. Although it does reproduce the character of the single-field GFEA spectra in many ways, the peak heights do not agree – a fact that is more apparent on a linear scale than a logarithmic one. In terms of a multi-field model, we can say that without the GFEA corrections, the prefactor of the polarization term does not pick up its correct frequency dependence, so the Stokes lines are artificially enhanced, and the anti-Stokes artificially suppressed.

Figure 2 shows a set of results from a single 10fs probe pulse at 397nm, traveling though 9cm of previously polarized D₂. This corresponds to the probe stage of an experiment where the gas had been prepared using a pair of nanosecond fields resulting in a medium polarization of $\rho_{12} = 0.025i$ on the 2993.57cm^{-1} ($\sim 90\text{THz}$) vibrational transition, e.g. as in the experiments of Gundry et.al. [13], who use a longer probe pulse of about 150fs. A Cauchy-type dispersion curve is incorporated into the simulations, but in the absence of good dispersion data for D₂, we use that for H₂ as it should be a good match. Note that although the polarization initial condition is fixed, our simulations do incorporate the response of the polarization to the probe pulses. The main spectral peaks agree well in the multi-field and single-field GFEA simulations, although as before the results differ at the edges where the intensities are very small compared to the main features. As for the previous situation, in the single-field SVEA simulation the Stokes and anti-Stokes lines are artificially enhanced or suppressed.

V. DISCUSSION

For simple systems, those (for example) with a single Raman transition driven by relatively long pulses, it will usually be most efficient to continue using a multi-field model. Single-field simulations require very fine time-resolution, so they are computationally expensive for pulses with many optical cycles. The spectral range of the numerical field is correspondingly broad, typically covering many Stokes and anti-Stokes lines.

In more complex situations, however, the single-field approach will outperform its multi-field counterpart. For example, if a Raman interaction is probed by a beam that does not

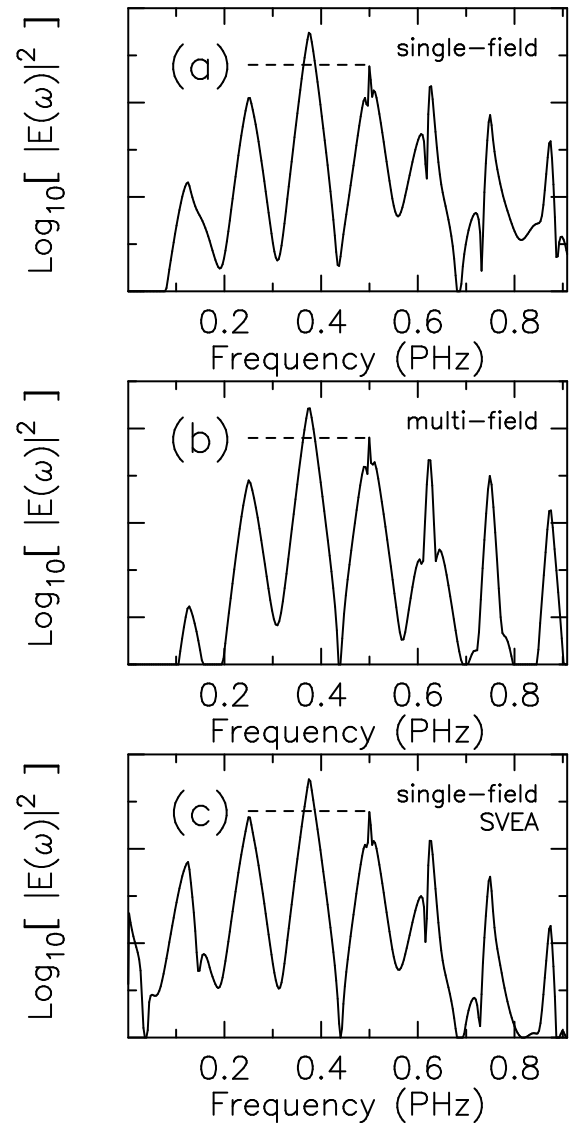


FIG. 1: Transient Raman generation using 17.5fs and 62.5f pump pulses as described in the text. Here we compares three simulation results: (a) single-field GFEA simulation, (b) multi-field simulation, and (c) single-field SVEA simulation. The dashed lines help compare the relative heights of the first Stokes and anti-Stokes peaks. The vertical scale is in arbitrary units.

lie on the frequency comb defined by the pumping beams (e.g. as in [13]), the multi-field approach will become much more complicated to implement. It will be necessary to define separate arrays for the pump and probe Raman “ladders” of Stokes and anti-Stokes lines, an issue that we avoided in section IV by replacing the pump stage of the process with an initial condition for the polarization. With a single-field model, the probe pulse and its Raman sidebands simply get superimposed on the overall spectrum, where they will be offset from the frequency ladder defined by the pump beams.

Another situation in which the multi-field model will run into difficulty is where there are multiple Raman resonances. Although the treatment in this paper has been restricted to

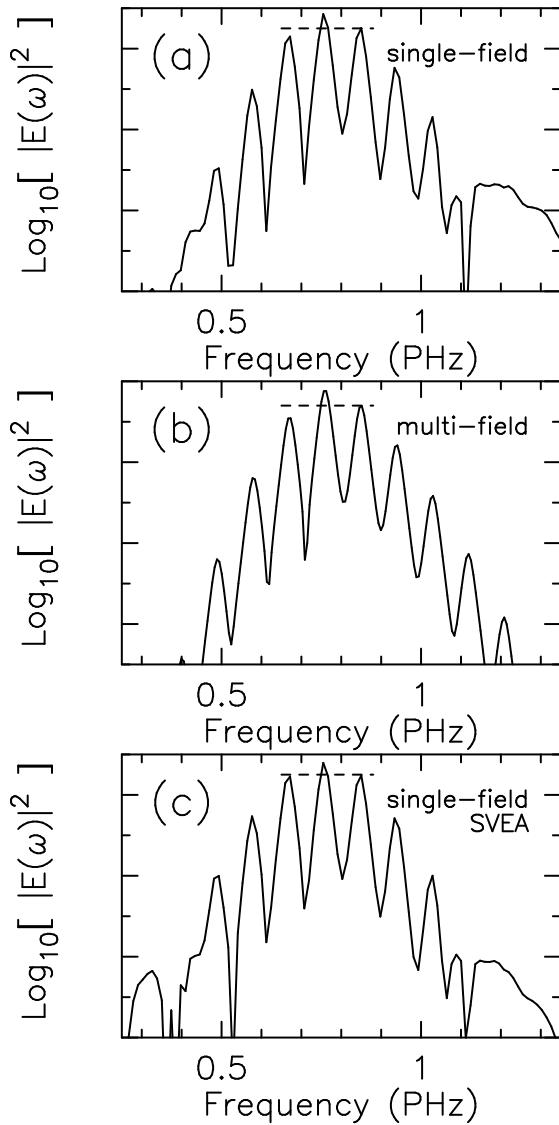


FIG. 2: 10fs probe pulse incident on a medium with an initial polarization of $\rho_{12} = 0.025i$. Here we compares three simulation results: (a) single-field GFEA simulation, (b) multi-field simulation, and (c) single-field SVEA simulation. The dashed lines help compare the relative heights of the first Stokes and anti-Stokes peaks. The vertical scale is in arbitrary units.

a simple two-level Bloch equation description of the Raman medium, additional Bloch equations can easily be added, even

if there are coupled multi-level interactions (as for example in [14]). It is only necessary to describe those transitions appropriately, and to modify the polarization terms acting on the propagating field. This procedure is considerably more difficult to handle in the multi-field case, which is based on field components separated by a particular Raman transition frequency. Additional Raman resonances complicate the theory; not only must extra detuning factors be added to the equations, but it is also necessary to work out which field component is nearest to each new driving term. With a wideband single-field model, on the other hand, any new sidebands or resonance effects appear automatically in the spectrum, and no special measures need to be adopted to handle them.

The usefulness of our single-field approach is not restricted to the Raman interaction described in this paper. It is not just more easily extended to more complex Raman materials involving e.g. multiple transitions than the standard multi-field model. It would be equally valuable for a near-degenerate optical parametric oscillator, or indeed any system where two or more field components start to overlap as the pump or probe pulses get shorter.

VI. CONCLUSION

We have considered how best to model the multi-frequency field in wideband Raman generation experiments. Rather than using multiple field envelopes, with one at each Stokes or anti-Stokes frequency, we instead use a single wideband field envelope. This requires that the field be propagated taking into account wideband effects, as described by either the SEWA theory of Brabec and Krausz [11], or the more general GFEA of Kinsler and New [8].

Our single-field approach has three crucial advantages. First, it includes more physics, even compared to a multi-field approach enhanced by adding GFEA corrections to the propagation of the field components. Secondly, it deals effortlessly with the complications of overlapping spectra that occur in the multi-field case. Thirdly, it allows for extra Raman transitions, and other molecular details to be included more easily than is possible for the multi-field model.

All of these factors ensure that our wideband single-field model not only extends the regime in which envelope-based methods can be utilised; but is also more versatile and places fewer restrictions on the kinds of Raman media that can be easily described.

[1] S. E. Harris, A. V. Sokolov, Phys. Rev. Lett. **81**, 2894 (1998).
 [2] A. V. Sokolov, D. R. Walker, D. D. Yavuz, G. Y. Yin, S. E. Harris, Phys. Rev. Lett. **87**, 033402 (2001).
 [3] K. Hakuta, M. Suzuki, M. Katsuragawa, J. Z. Li, Phys. Rev. Lett. **79**, 209 (1997).
 [4] E. Sali, K. Mendham, J.W.G Tisch, T. Halfmann, J.P. Marangos, Opt. Lett. **29**, 495 (2004).
 [5] R.M. Joseph and A. Taflove, IEEE Trans. Antennas Propag. **45**,

364 (1997)
 [6] J.C.A. Tyrrell, P. Kinsler, G.H.C. New, J.Mod.Opt. **52**, 973 (2005).
 [7] E. Sali, P. Kinsler, G.H.C. New, K. Mendham, T. Halfmann, J.W.G Tisch, J.P. Marangos, Phys. Rev. **A72**, 013813 (2005).
 [8] P. Kinsler, G.H.C. New, Phys. Rev. **A67**, 023813 (2003).
 [9] P.Kinsler, arXiv.org/physics/0212014.
 [10] A.P. Hickman, J.A. Paisner, W.K. Bischel, Phys. Rev. **A33**,



- 1788 (1986).
- [11] T. Brabec, F. Krausz, Phys. Rev. Lett. **78**, 3282 (1997).
- [12] P.Kinsler, arXiv.org/physics/0606112.
- [13] S. Gundry, M.P. Anscombe, A.M. Abdulla, E. Sali, J.W.G. Tisch, P. Kinsler, G.H.C. New, J.P. Marangos, Opt. Lett. **30**, 180 (2005).
- [14] H. Wallis, Phys. Rev. A **52**, 1441 (1995).
- [15] K.S. Syed, G.S. McDonald, G.H.C. New, J. Opt. Soc. Am B **17**, 1366 (2000).